Materials Advances

ROYAL SOCIETY OF CHEMISTRY

PAPER

View Article Online
View Journal | View Issue

Cite this: *Mater. Adv.*, 2022, 3, 6518

Understanding tyrosine self-assembly: from dimer assembly to magnetized fluorescent nanotubes embedded into PVA films†

Prabhjot Singh,‡[a] Rohit K. Sharma,[b] O. P. Katare[c] and Nishima Wangoo*[d]

Biomolecular self-assembly has emerged as a remarkable tool for the development of functional materials at biological interfaces. Considerable attention has been focused on amino acid-based tubular structures, such as protein (tubulin) microtubes and β-sheets containing diphenylalanine nanotubes, for their role in cognitive function and neurodegenerative disorders. Further, the unique photophysical properties displayed by single amino acid self-assembled structures may find novel applications in the field of bio-optoelectronics and biophotonics. However, the nanoscale crystallinity and its role in hierarchical self-assembly formation may lead to a distinctive path for a particular molecular system. In the quest to understand tyrosine nanoscale self-assembly, we have demonstrated that tyrosine forms microrod (TyrMR) structures *via* the multiple stacking of tyrosine nanotubes (TyrNTs), which are composed of tyrosine dimer assemblies (TyrDAs) as the basic unit. Further, we showed that the unique photoluminescence displayed by TyrMR structures can be tuned *via* the co-assembly of phenylalanine and thioflavin T dye. The photoactive TyrMRs were magnetized using ferrite nanoparticles to generate a binary nanocomposite, which was further embedded into a PVA thin film to produce a magneto-opto-active ternary nanocomposite. The fabricated ternary nanocomposite structure presented multifunctional features, such as nanocrystallinity, tunable photoluminescence, and a magnetic response, which may pave the way for the development of integrated functional materials with potential applications in multimodal optical imaging, bioimaging, and biophotonics.

Received 16th May 2022,
Accepted 3rd July 2022

DOI: 10.1039/d2ma00546h

rsc.li/materials-advances

Introduction

The fabrication of functional materials using bioinspired molecular motifs is at the forefront of material science research.[1] The vision, design and development of such materials can be conceptualized through molecular self-assembly.[2] Out of many bioinspired nanomaterials, peptide nanotubes have gained much attention in both physiology and material science owing to their pathological and functional characteristics, respectively.[3] Further, peptide nanotubes have shown potential as a functional material owing to their unmatched biochemical and thermal stability.[4] Compared to SWCNTs, peptide nanotubules can offer a wide range of interfacial interactions owing to the presence of exoskeleton functional groups, which may be useful for applications in biological environments.[5]

In recent years, amino acid and peptide nanotubes have been explored for applications in diverse areas, such as development of biomimetic enzymes, biosensors, piezoelectric nanomaterials, bioinspired semiconductors and drug delivery vehicles.[6–10] Apart from peptides, naturally occurring amino acids have also been utilized for the generation of well-defined nanostructures such as nanofibrils, nanotubes and nanoribbons.[11–15] The simplest amino acid, glycine, has been reported to exhibit non-centrosymmetric packing, which may be the reason for the polarity reversal that is responsible for its piezoelectric effect, which is comparable to the those of the best inorganic materials, such as lead zirconate titanate (PZT) and $BiFeO_3$.[7] Among aromatic amino acids, phenylalanine has been observed to form spontaneous nanofibril deposits, which affect neuron cells in a way that results in the loss of cognitive ability in phenylketonuria-affected patients.[12] On the other hand, phenylalanine nanostructures have also been investigated for

[a] *Centre for Nanoscience and Nanotechnology, Panjab University, Sector 25, Chandigarh-160014, India*
[b] *Department of Chemistry & Centre for Advanced Studies in Chemistry, Panjab University, Sector 14, Chandigarh-160014, India*
[c] *University Institute of Pharmaceutical Sciences, Panjab University, Sector 14, Chandigarh-160014, India*
[d] *Department of Applied Sciences, University Institute of Engineering and Technology, Panjab University, Sector 25, Chandigarh-160014, India. E-mail: nishima@pu.ac.in*

† Electronic supplementary information (ESI) available. See DOI: https://doi.org/10.1039/d2ma00546h

‡ Present address: Senior Secondary Residential School For Meritorious Students, Ludhiana, Punjab-141401, India.

the generation of functional nanomaterials for biomedical applications.[6] Recently, we have demonstrated that phenylalanine forms dimer assemblies as the basic constituent of the nanofibrillar network.[16] These nanofibrils also demonstrated unique photoluminescence, which may be due to quantum confined proton entrapment in clustered hydrogen bonds in phenylalanine dimers.[16–18] Despite these unique photophysical properties of amino acid-based structures, not much progress has been made in the optimization of the biomolecular nanomaterials for their applications at biological interfaces.

Subsequently, tryptophan and tyrosine have been reported to form self-assembled nanotubes.[19] Similar to tubulin microtubules, tyrosine nanostructures have also been reported to self-assemble into nanotubes of size 25–50 nm in diameter, consisting of a dimer assembly as their basic constituting unit.[18] Interestingly, a characteristic transformation of MTs to nanofibrillary entangles has been suggested to be linked with loss of cognitive ability, as in the case of Alzheimer's disease.[20,21]

Apart from pathological relevance, the autofluorescence as well as the ferroelectric properties of self-assembled tyrosine have projected it to be a promising candidate for applications in diverse areas, such as biophotonics and bio-optoelectronics. However, a detailed molecular-level hierarchal self-assembly mechanism is yet to be discussed. Thus, an understanding of the nanocrystallinity involved in tyrosine self-assembly may expedite the development of biophotonic functional materials using simple biomolecules.

Keeping this in mind, herein, we report the self-assembly mechanism for tyrosine in aqueous medium from dimeric assembly (TyrDA) to microrod (TyrMRs) structures *via* the formation of nanotubes (TyrNTs). The morphological and photoluminescence properties were recorded at various stages of the tyrosine self-assembly process. Further, the PL profile of tyrosine was modulated using co-assembly with phenylalanine and molecular dyes. So far, most of the reports on tyrosine self-assembly have focused on the amyloid formation and its related toxicity. Apart from that, tyrosine self-assembled materials have also been tested for their elastic,[22] charge transport, and photowaveguiding properties.[18] Yet, the causal sequence from molecular interactions to the formation of TyrMR crystals has not been studied in much detail. Thus, the work in this paper points towards the hierarchical mechanism as well as its relation to the nanocrystallinity and autofluorescence of tyrosine nanostructures, which may pave the way for nanoscale biophotonic applications. Further, this is the first time that single amino acid intrinsic PL has been tuned within the visible spectral region. The modulation in the photoactive properties using the molecular co-assembly mechanism may also have broad implications in the design and development of future biophotonic materials.

Further, the generated TyrMRs were magnetized using iron nanoparticles (FeNPs) to generate a photoluminescent binary nanocomposite. Finally, the FeNPs:TyrMRs composite was embedded into PVA thin film to produce a ternary nanocomposite. The TyrMRs-based ternary nanocomposite displayed multifunctional characteristics, such as nanocrystallinity, tunable photoluminescence, and the ability to co-assemble, which renders it an excellent candidate for the development of integrated functional materials with potential applications in multimodal optical imaging, bioimaging, and bio-photonics.

Results and discussion

Self-assembly and morphological analysis

Initially, tyrosine solutions were prepared at varying concentrations ranging from 1 mg mL^{-1} to 5 mg mL^{-1} (above its saturation point in water). The self-assembly of tyrosine at this elevated concentration was obtained using thermal treatment for 5 minutes at 90 °C followed by room temperature incubation for 1 hour. After 1 hour, tyrosine was observed to form rod-like microcrystals in water within the concentration range of 3 mg mL^{-1} to 5 mg mL^{-1}. This result indicated the occurrence of concentration-dependent bottom-up self-assembly from tyrosine molecules to form microscale structures. Further, the morphological analysis of tyrosine self-assembled structures at 1 mg mL^{-1} and 5 mg mL^{-1} concentrations was carried out *via* horizontal and vertical surface visualization using FESEM images. The tyrosine self-assembly analysis at 5 mg mL^{-1} showed the formation of microrod structures of ~3 μm width with a high aspect ratio.

Intriguingly, these microcrystals were observed to be formed by the multiple stacking of nanodimensional layers arranged in an ordered fashion [Fig. 1(a and b)]. On the other hand, the tyrosine self-assembly at 1 mg mL^{-1} displayed the formation of a distinct tubular structure with diameter of 40–50 nm with extended longitudinal order [Fig. 1(c and d)]. However, the desired nanotube dispersity may be achieved by controlling many factors, such as initial tyrosine concentration, solvent system, pH and surface charge density on the nanotubes.

This nanotubular structure showed good size correlation with the nanodimensional layered morphology, as observed in the case of tyrosine self-assembly at a concentration of 5 mg mL^{-1}. The stacked tyrosine nanotubes that are approximately 50 nm in diameter appear to be the constituent units of the tyrosine microrod structures with a width of ~3 μm, as indicated by the FESEM micrographs. Thus, the formation of an individual nanodimensional tubular structure as a core unit, which then grows into the suspended microrods at elevated concentrations, shows a structural hierarchy in tyrosine self-assembly formation.

Investigating quantum confined nanocrystalline regions in tyrosine self-assembled structures using optical spectroscopy

The spectroscopic analysis of tyrosine was performed in aqueous medium to understand the mechanism behind the bottom-up molecular self-assembly. For this purpose, aqueous tyrosine solutions were prepared at different concentrations ranging from 0.0005 mg mL^{-1} to 5 mg mL^{-1}, where concentrations beyond 0.5 mg mL^{-1} were prepared by thermal treatment of the aqueous solution prior to the spectroscopic analysis. The UV-vis spectra of the aqueous solutions displayed a

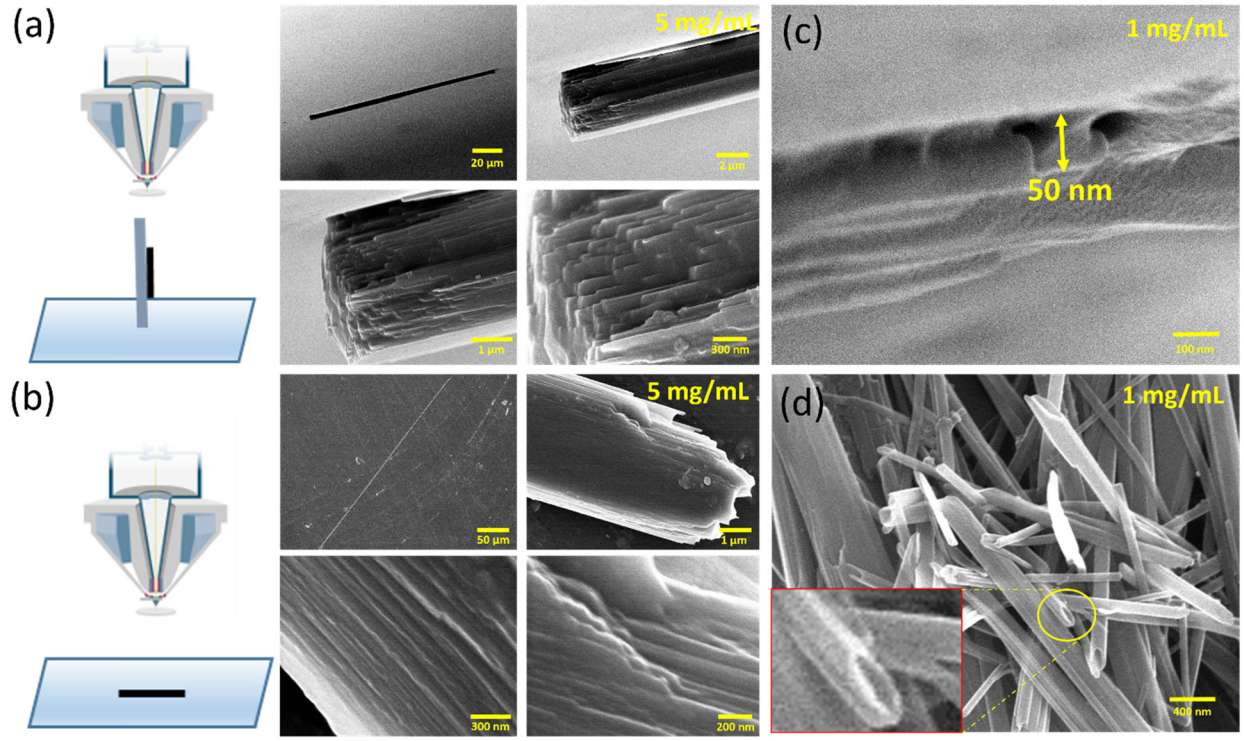

Fig. 1 FESEM images displaying tyrosine self-assembled structures at 5 mg mL^{-1} (a) with vertical inclination and (b) on a horizontal surface, and at 1 mg mL^{-1} (c) with vertical inclination and (d) on a horizontal surface.

concentration-dependent increase in the absorbance peak at 274 nm. In the case of tyrosine, the shape of the UV-vis spectral peak for tyrosine at 274 nm was observed to broaden as compared to the spiked pattern displayed by phenylalanine in our earlier report.[16] The broadening of the UV-vis peak may be due to the hydroxyl functionalization of the phenyl ring [Fig. S1, ESI†]. In addition to this, an increase in the concentration from 1 mg mL^{-1} to 5 mg mL^{-1} resulted in a corresponding increase in the absorbance between 300 nm and 900 nm, which may be due to the formation of an ordered aggregate assembly [Fig. 2(a)].[23]

Subsequently, the PL spectra for tyrosine solutions at concentrations ranging from 0.001 mg mL^{-1} to 1 mg mL^{-1} were analyzed at an excitation wavelength of 247.5 nm. The concentration-dependent spectral analysis displayed an increase in the PL intensity for the peak at 303 nm [Fig. 2(b)]. This unusual increase in PL intensity as a function of the increase in concentration contradicts the general quenching phenomena observed for fluorophores at higher concentrations.[24] Further, the PL emission also displayed a red shift along with the increase in the radiative intensity upon increasing concentration from 0.002 mg mL^{-1} to 0.004 mg [Fig. 2(c)]. The observation of unique absorption spectra for concentration-dependent tyrosine self-assembly indicates the formation of a J-type dimer with coupled exciton effects owing to inline transition dipoles.[23] The observed data were plotted as a straight line between Log(I_{max}) and Log(concentration) [Fig. 2(d)].

The absorbance spectra and unique narrow PL emission profile for tyrosine indicate the occurrence of confined nanocrystallinity in the tyrosine assembly structures.[25] Thus, the size of the tyrosine confined structure was estimated using a zero dimensional quantum well model.[26] From optical analysis, the exciton binding energy (E_{ex}^{QD}) was calculated to be 0.071 eV using the breaking of the exciton at 244 nm and the phononless band at 247.5 nm. Subsequently, the radius of the tyrosine confined structure using 1.33 as the refractive index of the aqueous tyrosine solution was estimated to be equal to 0.60 nm [eqn (S1), ESI†]. The radius of the tyrosine confined structure (0.60 nm) obtained by the above analysis was found to be much larger than the radius of the tyrosine monomer. This may be owing to the formation of an oligomer state to form the tyrosine confined structure. This correlates with the unique PL optical signal obtained for the tyrosine self-assembly, which indicates the formation of a J-type coupled dimer.

Composition analysis of tyrosine confined assembly structures using MS and DFT studies

The composition of the tyrosine assembly was determined using ion trap mass spectrometry (ITMS) with and without prior thermal treatment of the aqueous solution. The results obtained displayed m/z peaks for [2M + H] at 363; [2M + $3NH_3$] at 413; and [2M + $3NH_3$ + Na] at 436, suggesting the independent existence of tyrosine dimer in aqueous medium [Fig. S2, ESI†]. In addition to this, the intermolecular interaction responsible for the stability of the tyrosine dimer assembly (TyrDA) structure was determined using density functional theory (DFT). The optimized structure of the tyrosine dimer assembly showed the existence of a hydrogen bond between zwitterionic units of two molecules [Fig. S3, ESI†]. Subsequent

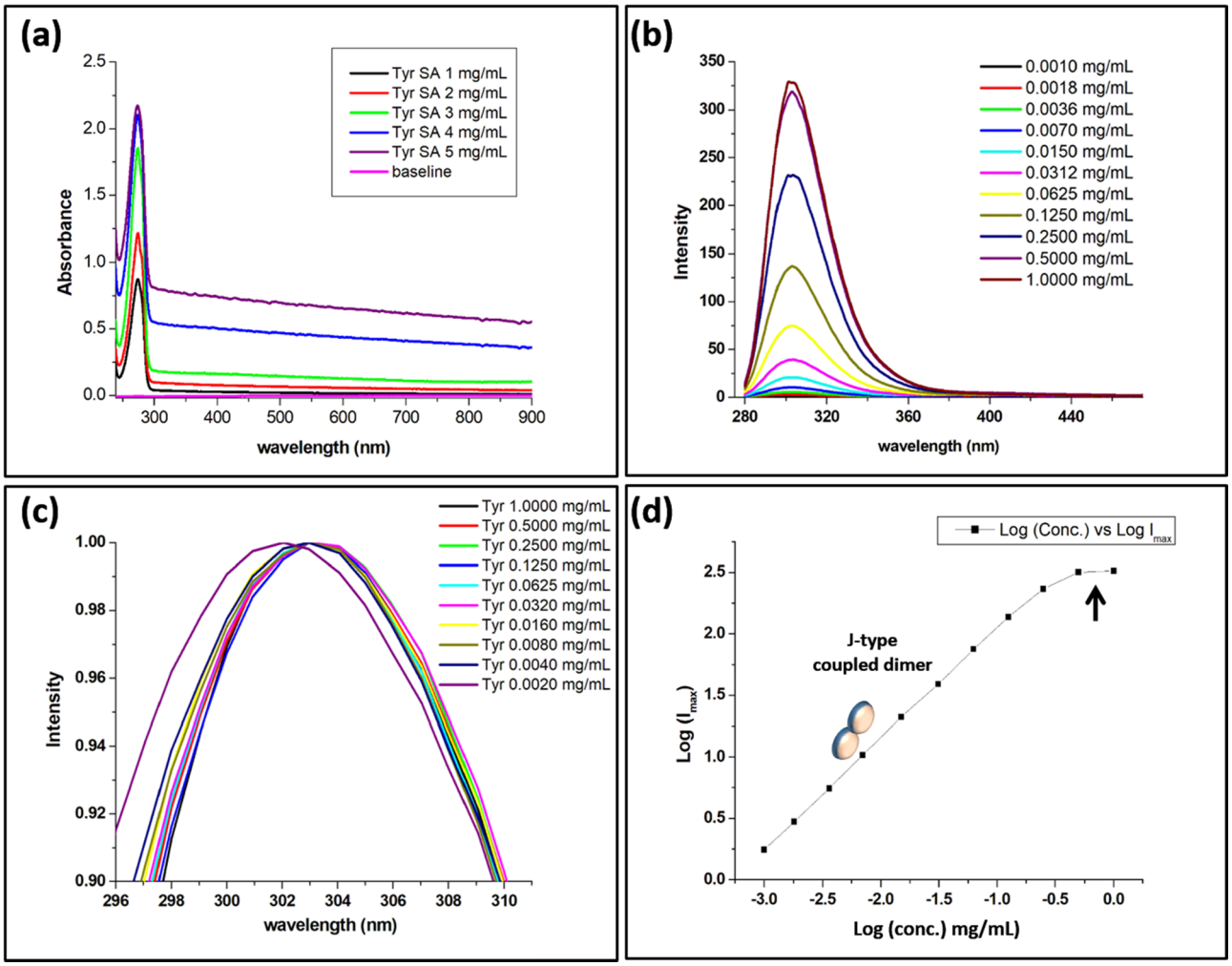

Fig. 2 (a) UV-Vis spectra of tyrosine self-assembly at different concentrations. (b) PL emission spectra of tyrosine at different concentrations. (c) The concentration-dependent red shift of tyrosine emission. (d) A plot of Log(I_{max}) *versus* Log(concentration).

evidence for the existence of the dimer assembly structure was generated using dynamic light scattering (DLS), which showed an intensity distribution particle radius of 0.50 nm in 1 mg mL^{-1} aqueous solution of tyrosine [Fig. S4, ESI†]. Thus, based on the correlating results obtained from the above investigations using optical, ITMS, DFT and DLS analysis, it is safe to say that the dimer assembly formation at the nucleation stage may be regarded as an integral part of the tyrosine self-assembly process.

Investigating the nanocrystallinity evolution of tyrosine self-assembled dimers using SAXS and XRD analysis

The nanodimensional structural organization of TyrDA was determined using SAXS analysis. For this purpose, the suspended microrod crystals of tyrosine self-assembly were extracted from water using an air drying method. The SAXS analysis for tyrosine microrods displayed a unique peak pattern in the scattering intensity with a broad peak at a q value of 4.91, which may correspond to the interacting dimer layered crystallinity of radial dimension 0.65 nm ($d = 2\pi/q$) [Fig. 3(a)]. The size of the tyrosine dimer calculated using optical analysis (0.60 nm) in the solution phase correlates fairly well with the size estimated using SAXS q peak (0.65 nm) in the solid phase. The occurrence of this peak in the SAXS pattern also confirms the existence of TyrDA as the core characteristic unit in the microscale self-assembled structures. Further, SAXS scattering also displayed an intense peak at the q value of 9.7, which may correspond to the tyrosine monomers with radial dimension of 0.32 nm. Notably, the two scattering peaks for the interlayer dimensions were nearly double in value, indicating that monomer tyrosine units may be weakly interacting to generate dimer crystallinity. Further, the SAXS pattern of the tyrosine self-assembled structures analyzed for space group determination displayed good fitting of scattering peaks with the *Fd3m* (face centred cubic lattice) space group with lattice parameter of 2.276 nm [Fig. S5, ESI†]. Consequently, from the obtained lattice parameter, the radius of the lattice point of the unit cell was calculated to be 0.80 nm [Calculation S3, ESI†]. Thus, the self-assembly phase transfer of tyrosine from solution to the solid state may be through soft inter-particle interactions

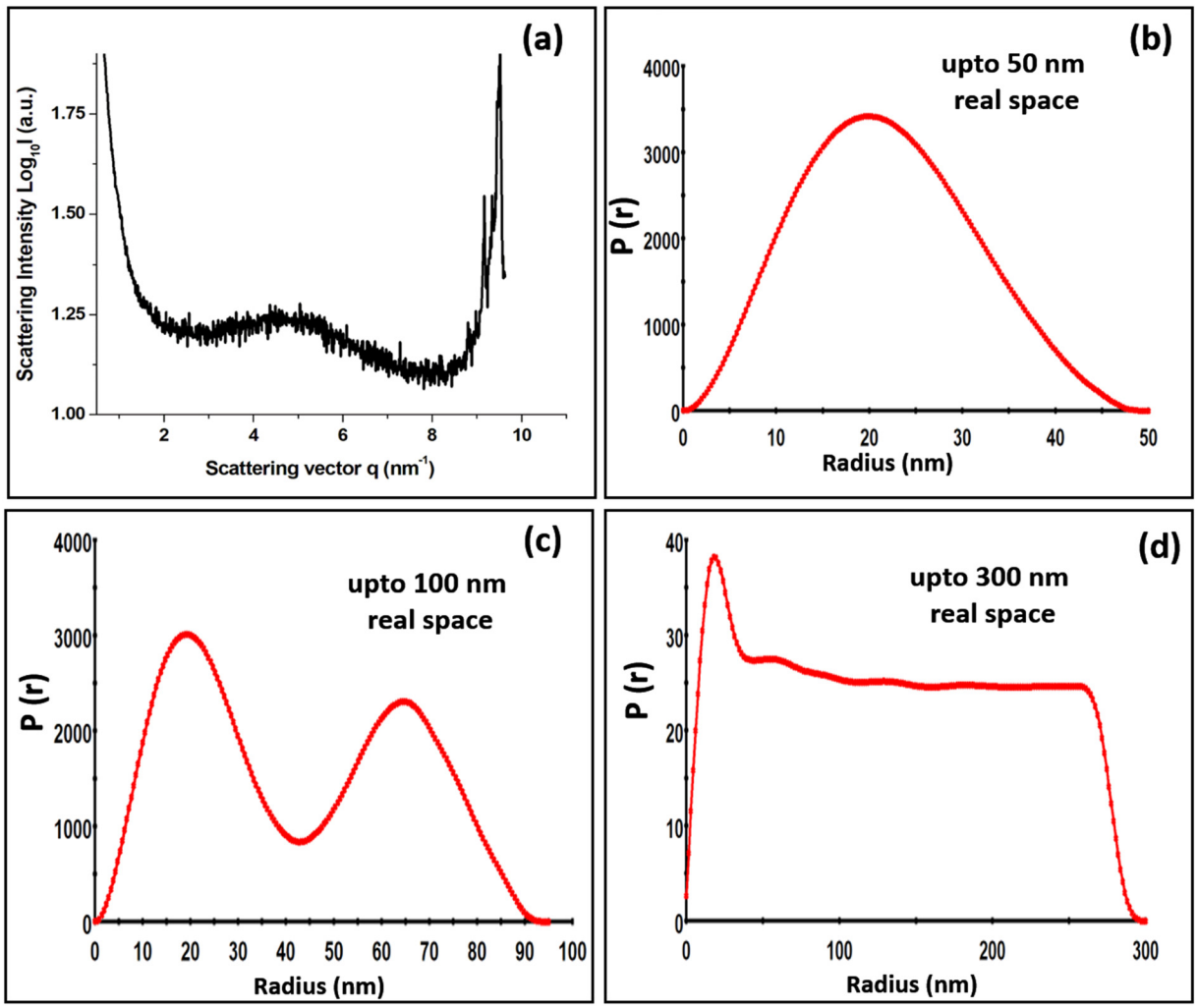

Fig. 3 (a) The SAXS scattering pattern of tyrosine self-assembled microstructures. PDDFs obtained *via* GIFT analysis of a tyrosine microrod assembly at real space limits of (b) 50 nm, (c) 100 nm, and (d) 300 nm.

between tyrosine dimer units. Further, the size and shape of tyrosine nanotubes constituting TyrMR was determined by GIFT analysis of the scattering pattern to obtain PDDFs at real space limits of 50 nm, 100 nm, and 300 nm [Fig. 3(b–d)]. The GIFT analysis generated a stable PDDF at 50 nm, which indicated the existence of a circular curvature of radius 20 nm (d = 40 nm) with slight ellipticity up to 47 nm, which may be due to the curvature of the nanotube, as depicted in the FESEM images [Fig. 3(a) and Fig. 1(c)]. Further, an increase in the real space limit up to 100 nm generated a stable PDDF, which depicted the formation of a secondary spherical nanostructure region with radius of 65 nm [Fig. 3(c)]. This intriguing result obtained from SAXS analysis of TyrMR illustrated the formation of multilayer tubular stacking while maintaining the individual nanotube crystallinity [Fig. 1(b)]. Further, the GIFT analysis at 300 nm real space limit yields long-range cylindrical structures with strong spherical distribution at radius 20 nm [Fig. 3(d)]. However, a sharp drop of PDDF at larger radius values indicates the existence of longitudinal order beyond 300 nm, which may extend up to micrometer scale as evidenced by the FESEM images.

The deconvolution of PDDF corresponding to 20 nm radius was done using DECON programme to obtain radial electron density, which displayed a 6 nm hollow region at the core followed by 14 nm radial electron density. This result correlates with the microscopic analysis depicting the occurrence of nanotube morphology constituting TyrMRs [Fig. 4(a)]. Further, the XRD pattern was obtained for TyrMR to estimate the particle size of the packed nanostructures. The XRD pattern showed a peak broadening as compared to the non-self-assembled tyrosine, which may be due to the formation of nanostructural dimensions. Thus, the Debye–Scherrer equation was employed to calculate the average size of the nanocrystallinity using the FwHm value for the most intense peak at 2θ = 18.07 in the XRD analysis [Fig. 4(b)]. The result obtained displayed a crystalline region of 13.33 nm, which matches closely with the outer layer dimension of the nanotube of 14 nm as obtained by DECON analysis of SAXS data [Calculation S4, ESI†].

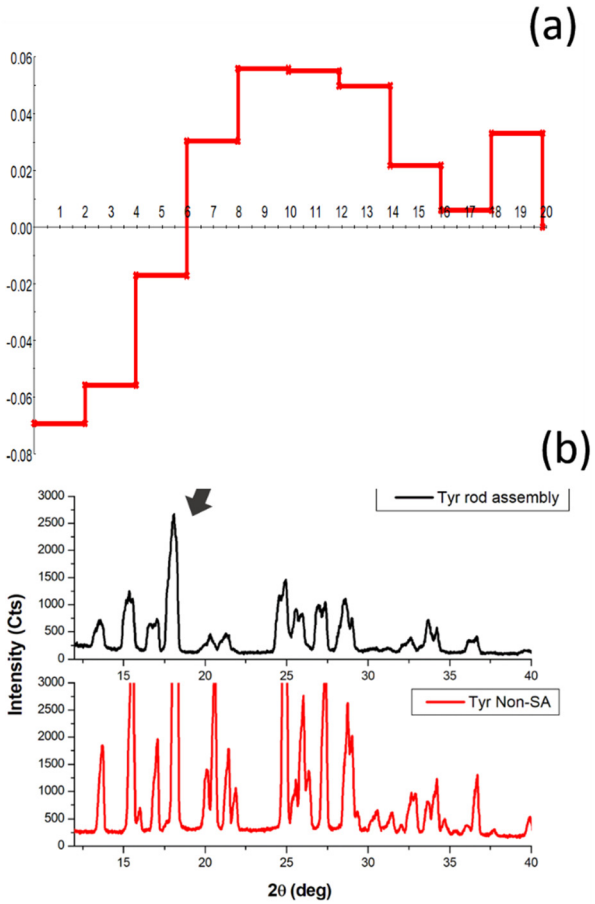

Fig. 4 (a) The deconvolution of the SAXS pattern using PDDF at the 50 nm real space limit using the DECON programme. (b) The XRD pattern of tyrosine self-assembled microrods and tyrosine non-self-assembled powder.

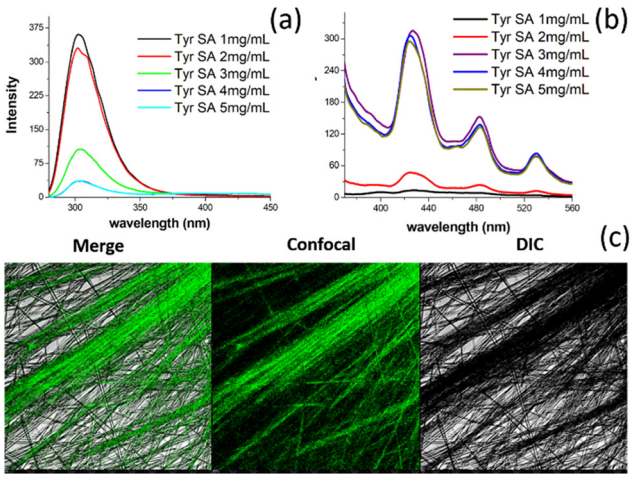

Fig. 5 (a) PL spectra of tyrosine self-assemblies at concentrations from 1 mg mL^{-1} to 5 mg mL^{-1} at excitation wavelengths of (a) 247.5 nm and (b) 350 nm. CLSM images of visible region light emission by self-assembled tyrosine tubular assemblies in (c) water and (d) ethanol extract.

Photoluminescence of tyrosine microrod self-assembled structures

The self-assembly analysis of tyrosine using various experimental and theoretical methods indicated the existence of a nano dimensional tubular assembly in the generated TyrMR, which may constitute tyrosine dimer assembly structure at the lattice point. The unique PL emission displayed by TyrMRs resulted in a lowering of the radiative intensity with increasing concentration from 1 mg mL^{-1} to 5 mg mL^{-1} at an excitation wavelength of 247.5 nm [Fig. 5(a)]. This may be due to the coupled lattice vibration upon clustering of TyrDA units into micro rod structures. However, the stacking process upon self-assembly of Tyr-DAs into the TyrMR structure gave rise to a unique PL peak pattern in the visible region located at 424 nm (FWHM ~ 32 nm), 483 nm (FWHM ~ 34 nm) and 530 nm (FWHM ~ 28 nm) at 370 nm excitation wavelength [Fig. 5(b)]. The emergence of such a narrow emission peak pattern may be attributed to the nanocrystalline-based quantum confinement in TyrDAs. Further, CLSM analysis was used for the visualization of visible region photoluminescence of TyrMR structures in the deposited phase [Fig. 5(c)]. The PL in the visible spectral range obtained by small molecular based self-assembled materials is rare and strongly desired to develop new biophotonic and bio-optoelectronic devices.

Based on the above experimental and theoretical analysis, we propose a stepwise mechanism for the formation of tyrosine self-assembled structures from TyrDAs to TyrMRs through the formation of TyrNTs [Fig. 6]. Specifically, we demonstrated that the tyrosine dimer assembly structures (TyrDAs) act as the basic constituent in the solution phase assembly process, which upon increasing the concentration lead to the formation of tyrosine nanotubes (TyrNTs) through the β-sheet secondary structure. A further increase in concentration allows TyrNTs to take up aligned orientation to form TyrMR structures of high aspect ratio. It is pertinent to mention here that the nanocrystallinity of TyrNT remains preserved during the formation of TyrMR, as evident by the SAXS analysis and PL spectra. However, the characteristic PL peak of the TyrDA structure showed a decrease in PL emission, which may be due to vibronic coupling of TyrDAs during phase transfer.

Co-assembly-based tuning of TyrMR photoluminescence

TyrMR co-assembly with molecular dyes. The tyrosine molecular assemblies have displayed the propensity to go through β-sheet structure for the formation of supramolecular nanotubes.[15,22,27,28] The formation of these β-sheet secondary structures was confirmed by the unique spectral signal obtained by the binding of specific molecular dyes such as thioflavin T (ThT) and Congo red (CR). Thus, we investigated the modulation in the visible region PL of TyrMRs in the presence of ThT and CR dyes. For this purpose, freshly prepared tyrosine self-assembled micro rods were generated and the suspension of TyrMRs was then co-assembled with ThT and CR at 1.5 mol% concentration as compared to tyrosine. The resulting solutions were centrifuged and the PL spectra of the redispersed TyrMR:dye co-assembled structures were recorded

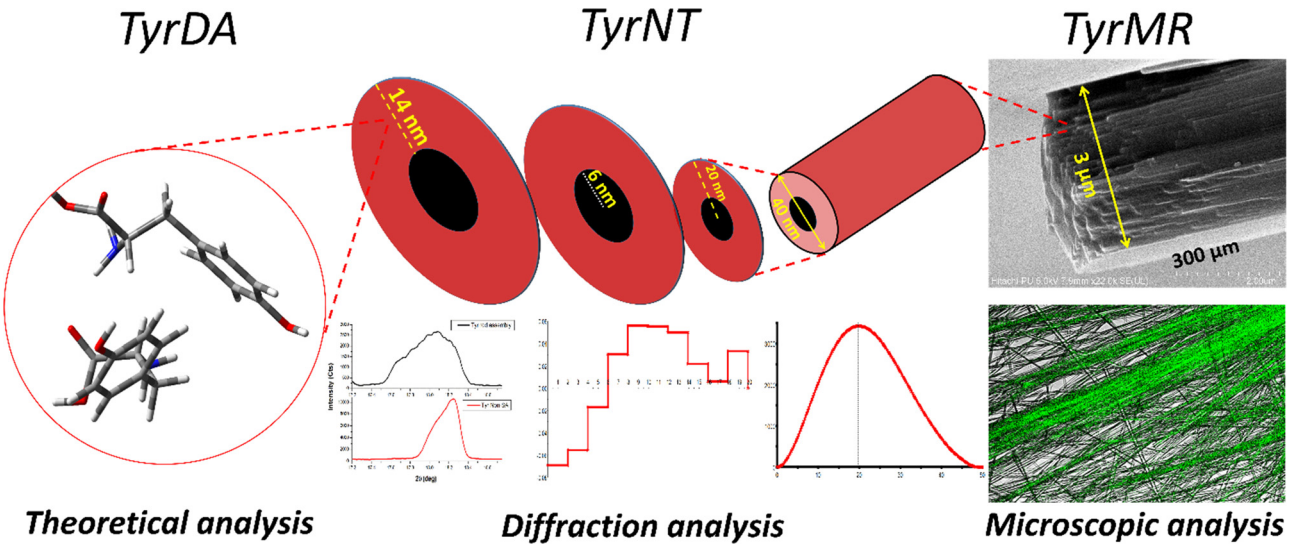

Fig. 6 A pictorial correlation of tyrosine nanocrystalline domains including a tyrosine dimer assembly (TyrDA), tyrosine nanotube (TyrNT), and tyrosine microrod (TyrMR) using theoretical, diffraction, and microscopic methods.

at an excitation wavelength of 350 nm. The TyrMR:ThT spectra indicated the loss of radiative intensity for the TyrMR peak at 424 nm, whereas the intensity of the TyrMR PL peaks at 484 nm and 529 nm remained unchanged [Fig. 7(a and b)].

Similarly, PL spectra of TyrMR:CR co-assembled structures displayed a sharp decrease in the intensity of peaks located at 484 nm and 529 nm. However, the PL peak located at 424 nm displayed moderate lowering in intensity. The results obtained

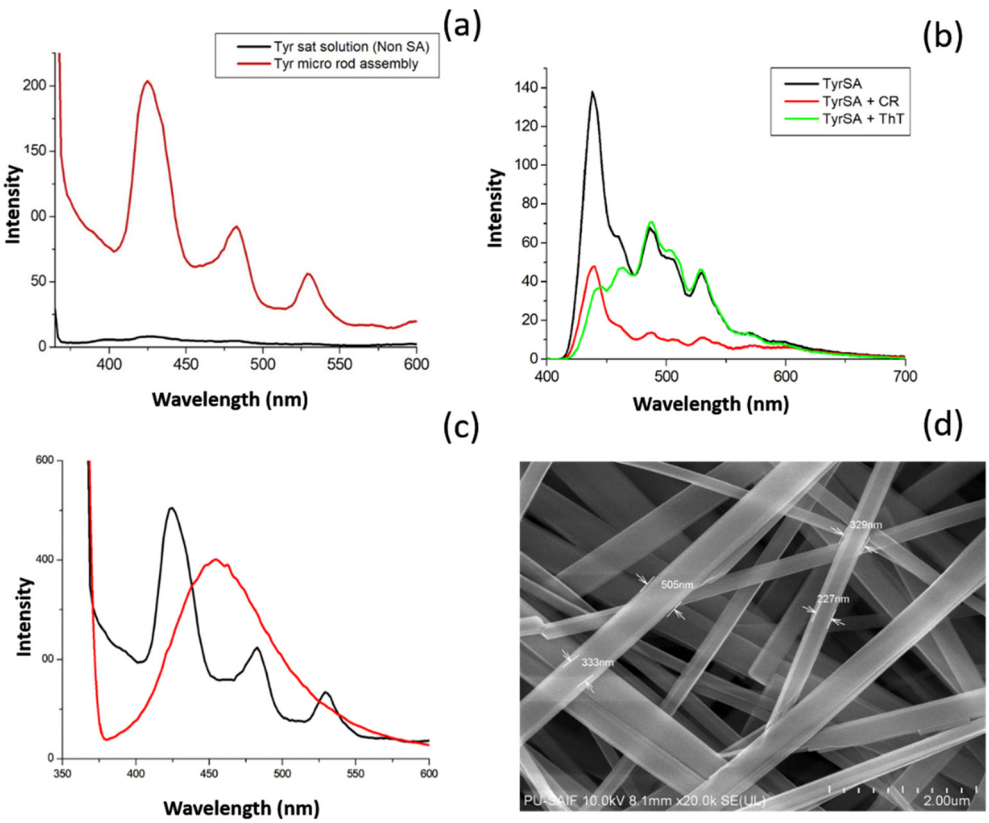

Fig. 7 (a) PL spectra of saturated tyrosine solution at 1 mg mL^{-1} without TyrMR assemblies and TyrMR structures at an excitation wavelength of 350 nm. (b) PL emission of TyrMR:dye co-assembled structures compared to only TyrMR self-assembly at an excitation wavelength of 350 nm. (c) PL spectra of TyrMR and TyrMR:phenylalanine co-assembly structures at an excitation wavelength of 350 nm. (d) FESEM images of TyrMR and TyrMR:phenylalanine co-assembled structures.

indicate specific binding of ThT and CR molecules to the tyrosine nanotubes. The variation in the lowering of the PL displayed by the different TyrMR:dye co-assembly structures may be due to the varying magnitude of the molecular interactions between the dye molecules (ThT and CR) and the different regions of the tyrosine supramolecular structures.

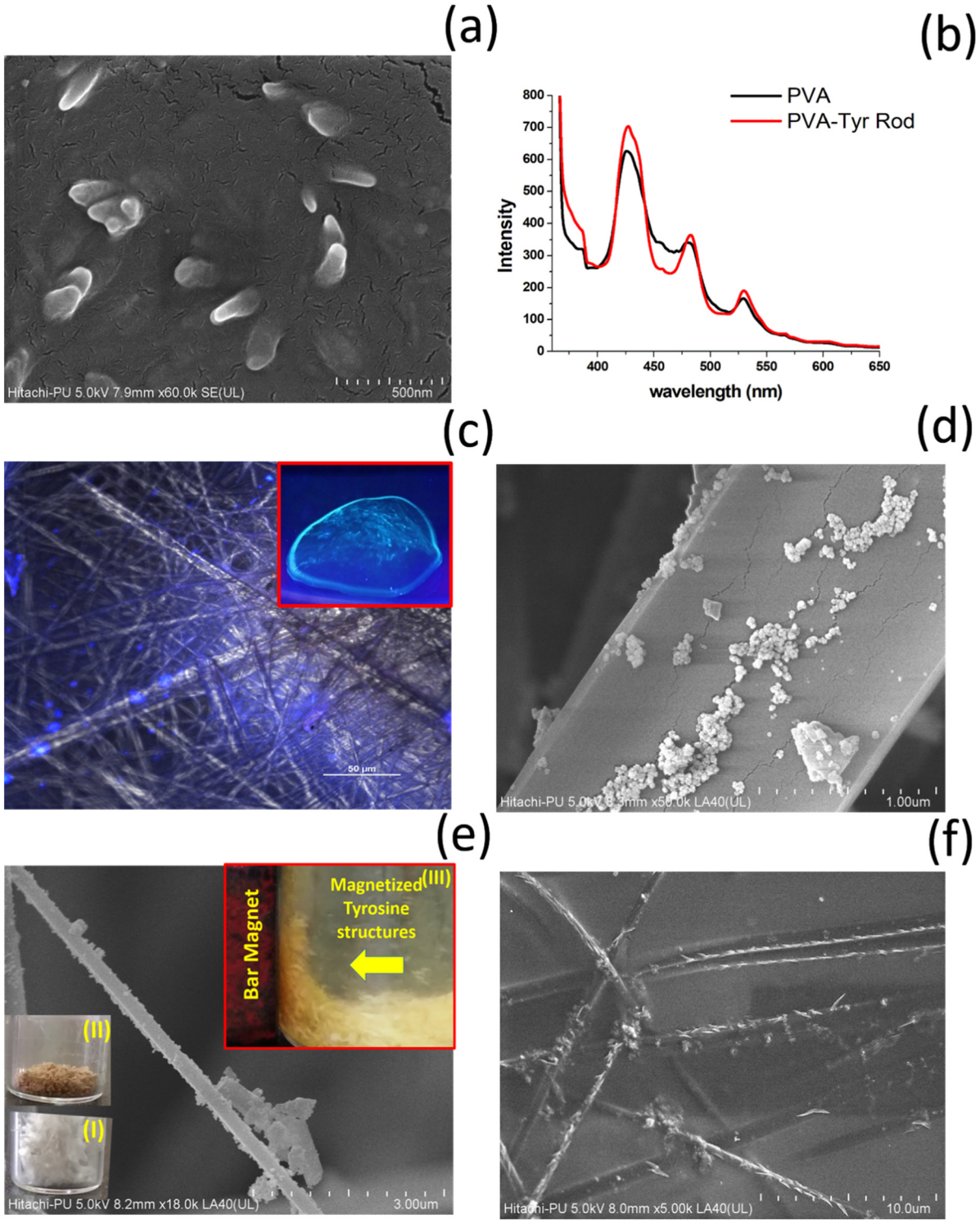

Fig. 8 (a) An FESEM image of the TyrMR:PVA binary nanocomposite. (b) PL emission spectra of TyrMR and the TyrMR:PVA binary nanocomposite at an excitation wavelength of 350 nm. (c) A CLSM image showing PL from the stable TyrMR nanocomposite in PVA thin films. (c, inset) A photographic image of TyrMR embedded into PVA thin film under UV illumination. (d and e) FESEM images displaying the stable FeNPs adsorbed onto the TyrMR self-assembled structures. (e, insets I and II) Air-dried TyrMRs and TyrMRs:FeNPs stored in a glass vial. (e, inset III) Magnetized Tyr:FeNps attracted towards a bar magnet from an aqueous suspension. (f) An FESEM image of a ternary nanocomposite including TyrMR:FeNPs inclusion into PVA thin film.

However, the exact explanation for this phenomenon requires further investigation. The modulation of the PL signal of the TyrMR:dye co-assembled nanocomposites may be a useful method for the development of tunable biophotonic nanomaterials.

TyrMR co-assembly with phenylalanine for the FRET-based tuning of PL. The amino acid self-assembled structures of tyrosine were observed to be similar to phenylalanine, in terms of their organizational inclination towards primary dimer units and secondary β-sheet structures.[16] Moreover, the similar molecular size and characteristic aromatic moiety common in both amino acids encouraged us to investigate the effect of phenylalanine:tyrosine co-assembly on the unique solution phase PL pattern displayed by TyrMRs.[29] The PL spectra of the phenylalanine:tyrosine co-assembly showed broadening effect on the narrow PL peaks exhibited by only TyrMRs in the visible region [Fig. 7(c)]. This indicated that the phenylalanine molecule may participate in the molecular-level interactions with tyrosine, causing peak broadening due to vibronic coupling. The FESEM analysis of the deposited phase phenylalanine:tyrosine co-assembled structures showed the formation of distinct nanofibrils [Fig. 7(d)]. This morphological analysis indicated the molecular-level packing of both molecules to yield well-defined dimensions to the self-assembled structures. The close molecular proximity between tyrosine and phenylalanine was further examined by the FRET based investigation for the PL peaks at 247.5 nm excitation wavelength. The PL of co-assembled state indicated a gradual red shift with the increase in tyrosine concentration [Fig. S6(a and b), ESI†].

Ternary nanocomposite: magnetized TyrMRs decorated with ferrite nanoparticles embedded into PVA thin films

So far, we have generated TyrMR structures that displayed unique PL features based on the nanoscale crystallinity. The stability and robust nature of the photoactive TyrMR structures in suspended aqueous medium rendered them as a potential candidate for the generation of bioinspired optoelectronic materials. The development of nanoscale optoelectronic devices mainly involves the incorporation of active photoactive material into thin films. Thus, the generated TyrMRs were used as a bridging substrate for the generation of active ternary nanocomposite using ferrite magnetic nanoparticles and PVA thin film.

For this purpose, firstly, the TyrMR nanostructures were incorporated into PVA thin films where PVA was used at 1 wt% concentration for the generation of the thin films. The resulting PVA solution was mixed with TyrMRs at 1 mg mL^{-1} as the final concentration followed by overnight air drying at 40 °C. The morphology of the generated binary nanocomposite displayed successful inclusion of tyrosine nanotubes into the PVA thin film [Fig. 8(a)]. This methodology may also be useful for restricting the size of the tyrosine crystallite in the nanotubular dimension upon transformation from solution to solid state. Further, the PL spectrum of PVA:TyrMR revealed that both PVA and TyrMR preserved their respective narrow emission peaks. However, the characteristic PL peak exhibited by the tyrosine self-assembly at ~303 nm when excited at 247 nm (absent in the PVA PL profile) displayed an increase in intensity, which may be due to the solid state clustering of tyrosine self-assembled units in the PVA film [Fig. S7, ESI†]. The PL of both

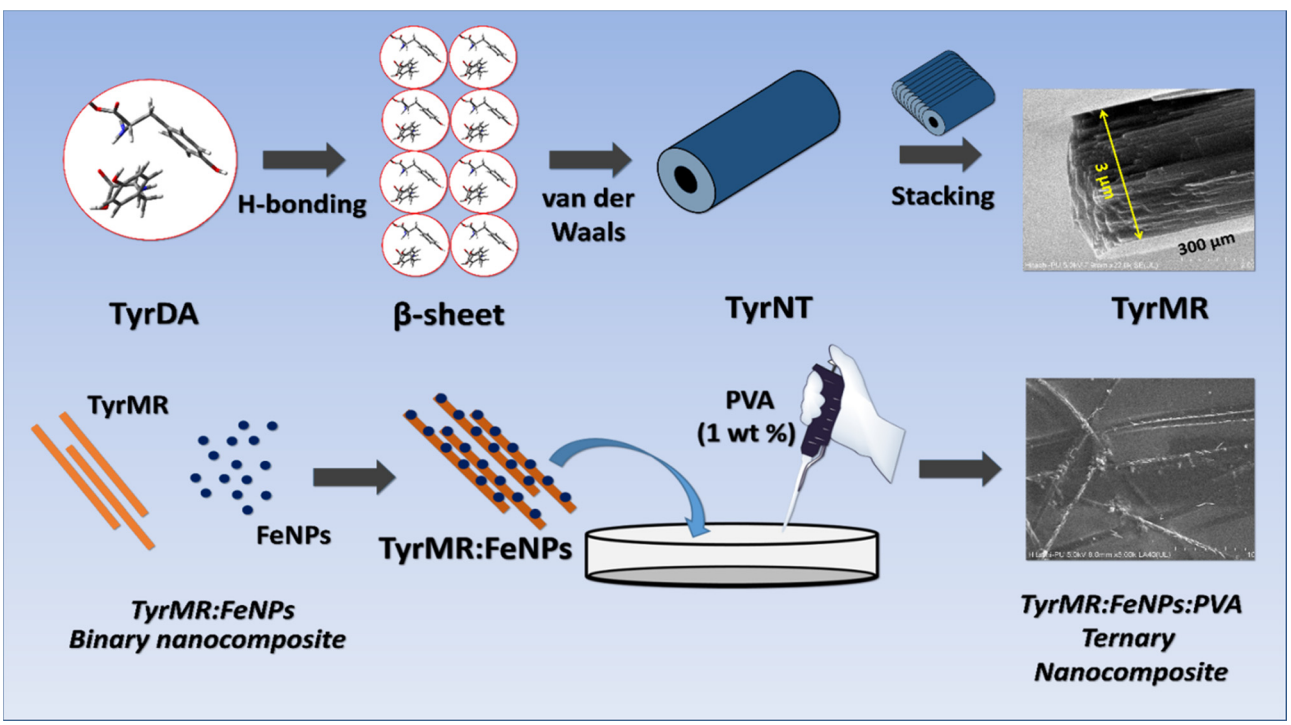

Scheme 1 A pictorial depiction of tyrosine self-assembly from TyrDA to a TyrMR structure *via* TyrNT and its fabrication into binary (TyrMR:FeNPs) and ternary (TyrMR:FeNPs:PVA) nanocomposites.

PVA and PVA:TyrMR nanocomposite at excitation wavelength of 350 nm displayed similar characteristic narrow peaks in the visible region located at 424 nm, 484 nm and 529 nm, which may be due to trapped proton confinement as observed earlier for various luminogens [Fig. 8(b)]. The visible region emission for PVA:TyrMR was also confirmed by UV illumination of the thin film [Fig. 8(c); inset] as well as PL emission using CLSM [Fig. 8(c)].

As a second step prior to the generation of the ternary nanocomposite, the generated TyrMRs were decorated with magnetically active ferrite nanoparticles (FeNPs), which may impart novel magneto-optical phenomena in the designed ternary nanocomposite material. For this purpose, initially, citrate-capped ferrite nanoparticles were synthesized using conventional methodology.[30] The generated ferrite nanoparticles (FeNPs) were purified using centrifugation, then analyzed by UV-vis and FESEM, which confirmed the successful synthesis of ferrite nanoparticles [Fig. S8 and S9, ESI†]. The synthesized FeNPs were then incubated for 6 hours with TyrMRs prepared at 3 mg mL^{-1}. After incubation, the composite material was dried and placed overnight in an air oven at 40 °C to obtain a light brown coloured fibrillar material [Fig. 8(e); insets I and II]. XRD analysis of the TyrMR:FeNPs composite displayed characteristic FeNP peaks, which indicated the retention of nanoscale stability for FeNPs [Fig. S10, ESI†]. Further, the nanoscale composite generated at the level of single TyrMR was also confirmed by FESEM analysis and EDS mapping [Fig. 8(d, e) and Fig. S11, ESI†]. The FESEM image clearly indicates the effective loading of FeNPs over TyrMR, which imparted strong magnetization, as indicated by the attraction of TyrMR:FeNPs towards a bar magnet in the suspended state [Fig. 8(e); inset III]. Therefore, photoluminescent TyrMRs containing TyrNTs were successfully magnetized and incorporated into PVA films to generate a ternary nanocomposite, as displayed in Scheme 1.

Conclusions

In this paper, we have presented an in-depth mechanism for the molecular assembly of tyrosine to form TyrMRs structures as a stable aqueous suspension. The TyrMRs, constituting stacked nanotubular units, were found to be composed of ordered TyrDAs. These TyrDAs displayed unique PL emission in the visible region in both suspended and deposited phases. The stability of tyrosine nanocrystallinity with its unique PL in an aqueous medium may open up various possibilities for relevant applications in biofluids. Further, TyrDA demonstrated the formation of a J-type transition dipole with an average radius of 0.65 nm, which may be suitable for obtaining piezoelectric properties. Further, the formation of a non-centrosymmetric dimer assembly in tyrosine nanotubules may also be investigated for application in ferroelectric materials. The unique ability of suspended TyrMRs to preserve nanotubular crystallinity was confirmed by using SAXS analysis, which showed the presence of two nanotubes under a TyrMR width of 100 nm. Further, DECON SAXS, and XRD analysis estimated the internal and external diameters of TyrNTs to be 13 nm and 50 nm, respectively, which correlated well with the FESEM analysis. The TyrMR model consisting of an ordered array of nanotubes may be developed as a suitable model for the investigation of quantum effect-based cognitive impairment in neurons.

The co-assembly of generated TyrMRs with phenylalanine and photoactive molecular dyes demonstrated the tuning of visible PL, which may be useful for the development of biophotonic devices. The photoactive TyrMRs were further decorated with FeNPs to generate a magnetically active binary nanocomposite. The immobilization of FeNPs over TyrMRs may also be used to generate stabilized magneto-biophotonic materials. Finally, TyrMR:FeNPs were embedded into PVA thin film for the generation of a ternary nanocomposite material. Interestingly, the intact nanoscale crystallinity and photophysical properties of the tyrosine self-assembled structures after the inclusion of FeNPs and PVA thin film can lead to the generation of nanocomposite materials with potential applications in multimodal optical imaging, bio-optoelectronics, and biophotonics. Intriguingly, the well-defined tyrosine nanotubes may also be used as an alternative model in place of microtubules for the study of 'Orch OR' theory in cognitive neuroscience. Furthermore, an in-depth understanding of the tyrosine self-assembly mechanism may be utilized to devise state-of-the-art strategies against disorders caused by metabolic amyloids and for biomedical applications, such as drug delivery and bioimaging.

Author contributions

Prabhjot Singh: Writing – original draft, investigation, methodology, conceptualization and experimentation; O. P. Katare: review and supervision, Rohit K. Sharma: manuscript editing and methodology; Nishima Wangoo: supervision, conceptualization, manuscript writing and review, overall supervision, research support.

Conflicts of interest

The authors declare that they have no known competing financial interests or personal relationships that could have appeared to influence the work reported in this paper.

Acknowledgements

This work was supported by Science Engineering and Research Board (SERB) of India grant no. ECR/2017/000874 and a DSTPURSE grant awarded to N. W. P. S. thanks University Grant Commission (UGC), India, for his senior research fellowship.

References

1 U. G. K. Wegst, H. Bai, E. Saiz, A. P. Tomsia and R. O. Ritchie, *Nat. Mater.*, 2015, **14**, 23–36.
2 P. Chakraborty and E. Gazit, *ChemNanoMat*, 2018, **4**, 730–740.
3 N. Kol, L. Adler-Abramovich, D. Barlam, R. Z. Shneck, E. Gazit and I. Rousso, *Nano Lett.*, 2005, **5**, 1343–1346.
4 L. Adler-Abramovich, M. Reches, V. L. Sedman, S. Allen, S. J. B. Tendler and E. Gazit, *Langmuir*, 2006, **22**, 1313–1320.
5 X. Gao and H. Matsui, *Adv. Mater.*, 2005, **17**, 2037–2050.
6 O. V. Makhlynets and I. V. Korendovych, *Nat. Catal.*, 2019, **2**, 949–950.
7 S. Guerin, A. Stapleton, D. Chovan, R. Mouras, M. Gleeson, C. McKeown, M. R. Noor, C. Silien, F. M. F. Rhen, A. L. Kholkin, N. Liu, T. Soulimane, S. A. M. Tofail and D. Thompson, *Nat. Mater.*, 2018, **17**, 180–186.
8 K. Tao, P. Makam, R. Aizen and E. Gazit, *Science*, 2017, **358**, eaam9756.
9 M. Yemini, M. Reches, E. Gazit and J. Rishpon, *Anal. Chem.*, 2005, **77**, 5155–5159.
10 M. Amit, S. Yuran, E. Gazit, M. Reches and N. Ashkenasy, *Adv. Mater.*, 2018, **30**, 1–13.
11 S. Perween, B. Chandanshive, H. C. Kotamarthi and D. Khushalani, *Soft Matter*, 2013, **9**, 10141–10145.
12 L. Adler-Abramovich, L. Vaks, O. Carny, D. Trudler, A. Magno, A. Caflisch, D. Frenkel and E. Gazit, *Nat. Chem. Biol.*, 2012, **8**, 701–706.
13 K. P. Nartowski, S. M. Ramalhete, P. C. Martin, J. S. Foster, M. Heinrich, M. D. Eddleston, H. R. Green, G. M. Day, Y. Z. Khimyak and G. O. Lloyd, *Cryst. Growth Des.*, 2017, **17**, 4100–4109.
14 P. Singh, S. K. Pandey, A. Grover, R. K. Sharma and N. Wangoo, *Mater. Chem. Front.*, 2021, **5**, 1971–1981.
15 P. Singh, S. K. Brar, M. Bajaj, N. Narang, V. S. Mithu, O. P. Katare, N. Wangoo and R. K. Sharma, *Mater. Sci. Eng., C*, 2017, **72**, 590–600.
16 P. Singh, N. Wangoo and R. K. Sharma, *Soft Matter*, 2020, **16**, 4105–4109.
17 D. Pinotsi, L. Grisanti, P. Mahou, R. Gebauer, C. F. Kaminski, A. Hassanali and G. S. Kaminski Schierle, *J. Am. Chem. Soc.*, 2016, **138**, 3046–3057.
18 W. Ji, B. Xue, Z. A. Arnon, H. Yuan, S. Bera, Q. Li, D. Zaguri, N. P. Reynolds, H. Li, Y. Chen, S. Gilead, S. Rencus-Lazar, J. Li, R. Yang, Y. Cao and E. Gazit, *ACS Nano*, 2019, **13**, 14477–14485.
19 D. G. Babar and S. Sarkar, *Appl. Nanosci.*, 2017, **7**, 101–107.
20 S. Hameroff and R. Penrose, *Phys. Life Rev.*, 2014, **11**, 39–78.
21 C. Pereira, *NeuroQuantology*, 2015, **13**, 232–239.
22 R. Y. Adhikari and J. J. Pujols, *Nano Select*, 2022, 1, DOI: 10.1002/nano.202200063.
23 N. J. Hestand and F. C. Spano, *Acc. Chem. Res.*, 2017, **50**, 341–350.
24 M. G. Kuzmin, N. A. Sadovskii, J. Weinstein and O. Kutsenok, *J. Chem. Sci.*, 1993, **105**, 637–649.
25 N. Amdursky, M. Molotskii, D. Aronov, L. Adler-Abramovich, E. Gazit and G. Rosenman, *Nano Lett.*, 2009, **9**, 3111–3115.
26 K. Tao, Z. Fan, L. Sun, P. Makam, Z. Tian, M. Ruegsegger, S. Shaham-Niv, D. Hansford, R. Aizen, Z. Pan, S. Galster, J. Ma, F. Yuan, M. Si, S. Qu, M. Zhang, E. Gazit and J. Li, *Nat. Commun.*, 2018, **9**, 1–11.
27 C. Ménard-Moyon, V. Venkatesh, K. V. Krishna, F. Bonachera, S. Verma and A. Bianco, *Chem. – Eur. J.*, 2015, **21**, 11681–11686.
28 D. Zaguri, T. Kreiser, S. Shaham-Niv and E. Gazit, *Molecules*, 2018, **23**, 1273.
29 C. Pommié, S. Levadoux, R. Sabatier, G. Lefranc and M. P. Lefranc, *J. Mol. Recognit.*, 2004, **17**, 17–32.
30 T. K. Mahto, A. Roy, B. Sahoo and S. K. Sahu, *J. Nanosci. Nanotechnol.*, 2015, **15**, 273–280.